Fundus Autofluorescence and Photoreceptor Cell Rosettes in Mouse Models

Erin Flynn,[1] Keiko Ueda,[1] Emily Auran,[1] Jack M. Sullivan,[2–5] and Janet R. Sparrow[1,6]

[1]Department of Ophthalmology, Columbia University, New York, New York, United States
[2]Research Service, Veterans Administration Western New York Healthcare System, Buffalo, New York, United States
[3]Department of Ophthalmology (Ross Eye Institute), University at Buffalo-SUNY, Buffalo, New York, United States
[4]Department of Pharmacology/Toxicology, University at Buffalo-SUNY, Buffalo, New York, United States
[5]SUNY Eye Institute, Buffalo, New York, United States
[6]Department of Pathology and Cell Biology, Columbia University, New York, New York, United States

Correspondence: Janet R. Sparrow, Department of Ophthalmology, Columbia University, 630 W 168th Street, New York, NY 10032; jrs88@columbia.edu.

Submitted: February 11, 2014
Accepted: June 28, 2014

Citation: Flynn E, Ueda K, Auran E, Sullivan JM, Sparrow JR. Fundus autofluorescence and photoreceptor cell rosettes in mouse models. *Invest Ophthalmol Vis Sci*. 2014;55:5643–5652. DOI:10.1167/iovs.14-14136

Purpose. This study was conducted to study correlations among fundus autofluorescence (AF), RPE lipofuscin accumulation, and photoreceptor cell degeneration and to investigate the structural basis of fundus AF spots.

Methods. Fundus AF images (55° lens; 488-nm excitation) and spectral-domain optical coherence tomography (SD-OCT) scans were acquired in pigmented *Rdh8*$^{-/-}$*/Abca4*$^{-/-}$ mice (ages 1–9 months) with a confocal scanning laser ophthalmoscope (cSLO). For quantitative fundus AF (qAF), gray levels (GLs) were calibrated to an internal fluorescence reference. Retinal bisretinoids were measured by quantitative HPLC. Histometric analysis of outer nuclear layer (ONL) thicknesses was performed, and cryostat sections of retina were examined by fluorescence microscopy.

Results. Quantified A2E and qAF intensities increased until age 4 months in the *Rdh8*$^{-/-}$*/Abca4*$^{-/-}$ mice. The A2E levels declined after 4 months of age, but qAF intensity values continued to rise. The decline in A2E levels in the *Rdh8*$^{-/-}$*/Abca4*$^{-/-}$ mice paralleled reduced photoreceptor cell viability as reflected in ONL thinning. Hyperautofluorescent puncta in fundus AF images corresponded to photoreceptor cell rosettes in SD-OCT images and histological sections stained with hematoxylin and eosin. The inner segment/outer segment–containing core of the rosette emitted an autofluorescence detected by fluorescence microscopy.

Conclusions. When neural retina is disordered, AF from photoreceptor cells can contribute to noninvasive fundus AF images. Hyperautofluorescent puncta in fundus AF images are attributable, in at least some cases, to photoreceptor cell rosettes.

Keywords: light, retinal degeneration, retina, retinal pigment epithelium, lipofuscin, bisretinoid

The disabling of reactive all-*trans*-retinaldehyde after its release from photoisomerized visual pigment depends, in part, on its transfer to the cytosolic compartment of photoreceptor outer segment discs by the ATP-binding cassette (ABC) transporter ABCA4,[1–4] followed by nicotinamide adenine dinucleotide phosphate (NADPH)-dependent reduction to all-*trans*-retinol by retinol dehydrogenase (RDH) activity.[5,6] Several RDH enzymes have been identified in photoreceptor cells, including retinol dehydrogenase 8 (RDH8), which is located within outer segments,[7] and retinol dehydrogenase 12 (RDH12), which can reduce all-*trans*-retinal in inner segments.[8] Thus far, mutations in RDH8 have not been shown to confer retinal disease in humans; the phenotype in mice is characterized by delayed clearance of all-*trans*-retinal and modestly enhanced formation of the all-*trans*-retinal adduct A2E.[9,10] In humans RDH12 mutations are associated with a severe autosomal recessive retinal dystrophy characterized by severe macular atrophy.[11,12] Although *Rdh12*$^{-/-}$ mice accumulate levels of A2E that are less pronounced than in *Rdh8*$^{-/-}$ mice,[10,13] the *Rdh12*$^{-/-}$ mice are more susceptible to light-induced photoreceptor cell degeneration.[14]

As noted above, an important consequence of inadequate handling of all-*trans*-retinal is the formation of all-*trans*-retinal-adducts that accumulate with age as bisretinoid lipofuscin in RPE cells. The bisretinoid of RPE lipofuscin is not produced in RPE; rather it forms in photoreceptor cells. The availability of vitamin A aldehyde for reaction with phosphatidylethanolamine drives the formation of the bisretinoids such as A2E; these fluorophores eventually accumulate as lipofuscin in the RPE. This pathway is reflected in the *Abca4*$^{-/-}$ (ATP-binding cassette transporter 4 null mutant) mouse, wherein escalating levels of bisretinoid are present because translocation of retinaldehyde across the photoreceptor disc membrane is inadequate to clear these reactive aldehydes.[1–3] The accumulation of RPE bisretinoids is accompanied by photoreceptor cell degeneration.[15] These mechanisms are further exemplified in the *Rdh8*$^{-/-}$*Abca4*$^{-/-}$ double knockout mouse wherein the deficiency in *Abca4* is augmented by the absence of Rdh8 and bisretinoid levels are elevated as compared with the single knockout *Abca4*$^{-/-}$ mice.[10]

In histological material, the retinae of *Rdh8*$^{-/-}$*/Abca4*$^{-/-}$ mice present with photoreceptor cell rosettes, deformations in which photoreceptor cells become circularly arranged with their

inner and outer segments directed centrally.[16] Rosette-like formations within the degenerating retina of other animal models of retinal degeneration also have been described[17,18]; included in this group are mice homozygous for the retinal degeneration 8 (rd8) mutation in *Crb1*.[19] Based on work using a mouse model of retinal detachment, we recently presented evidence indicating that histologically visible rosettes may correspond to autofluorescent puncta observed in flat-mounted retina and by confocal fluorescence scanning laser ophthalmoscopy.[20] Other mouse models of retinal degeneration also exhibit autofluorescence (AF) spots when imaged in flat-mounted retina or by scanning laser ophthalmoscopy (SLO).[21–23] However, correspondence between autofluorescent puncta and photoreceptor cell rosettes has not always been demonstrated and the source of the AF has remained puzzling.[24]

Here we have used *Rdh8*$^{-/-}$*/Abca4*$^{-/-}$ mice to address issues related to the formation, detection, and impact of RPE lipofuscin, the latter being the principal source of the inherent emission that is imaged noninvasively by confocal SLO (cSLO). Accordingly, we investigated the correspondence between fundus AF and the age-related accumulation of RPE lipofuscin and the temporal correlations between fundus AF and photoreceptor cell degeneration. We also examined the structural underpinnings of autofluorescent fundus spots by probing for correspondence among images acquired as fundus AF, spectral-domain optical coherence tomography (SD-OCT), and light and fluorescence microscopy.

Methods

Mice and Genotyping

Albino *Abca4/Abcr* null mutant mice (*Abca4*$^{-/-}$),[25] and pigmented *Rdh8*$^{-/-}$*Abca4*$^{-/-}$ mice (gift from Krzysztof Palczewski, Case Western Reserve University, Cleveland, OH, USA) were homozygous for Rpe65-Leu450. Wild-type mice (C57BL/6N, Charles River Laboratory, Wilmington, MA, USA; C57BL/6J, Jackson Laboratory, Bar Harbor, ME, USA) were Rpe65-450Met. The *Rdh8*$^{-/-}$*Abca4*$^{-/-}$ and C57BL/6N mice were homozygous for the rd8 mutation in *Crb1*.[26] Animals were housed under 12-hour on-off cyclic lighting with in-cage illuminance of 30 to 80 lux or 10 lux (C57BL/6N). After mice were euthanized and after enucleation, murine eyes were extracted for HPLC analysis or were processed for histology. Mouse DNA was PCR-amplified with primers to detect the following: targeted deletion of *Abca4,* 5′-CCACAGCACACATCAGCATTTCTCC-3′ (forward) and 5′-TGCGAGGCCAGAGGCCACTTGTGTAGC-3′ (reverse) (455-bp product indicated targeted deletion); Rpe65 Leu450Met variant, 5′-ACCAGAAATTTGGAGGGAAAC-3 (forward) and 5′-CCCTTCCATTCAGAGCTTCA-3 (reverse) (180- and 365-bp bands after MwoI restriction enzyme digestion indicated the leucine variant)[25,27]; Rdh8 null allele, 5′-tccgccttggaaacctgagccagaag-3′ (forward) and 5′-tgcgaggccagaggccacttgtgtagc-3′ (reverse)[9]; *rd8* mutation in *Crb1*, 5′-GTGAAGACAGCTACAGTTCTGATC (forward 1) and 5′-GCCCCTGTTTGCATGGAGGAAACTTGGAAGA CAGCTACAGTTCTTCTG (forward 2) and 5′-GCCCCATTTGCA CACTGATGAC (reverse) (450-bp product indicated the rd8 mutation).[19]

The research was approved by the Institutional Animal Care and Use Committee and was performed in accordance with the ARVO Statement for the Use of Animals in Ophthalmic and Visual Research.

Acquisition and Analysis of Fundus AF SD-OCT Images

Mice were anesthetized with an intraperitoneal injection of ketamine (100 mg/kg) and xylazine (10 mg/kg) and pupils were dilated with 1% tropicamide and 2.5% phenylephrine (Akorn, Inc., Lake Forest, IL, USA). Corneal desiccation was reduced by topical application of GenTeal Liquid Gel (Novartis, East Hanover, NJ, USA).[15] The mouse was positioned on a custom-made platform and body temperature was maintained with a heating blanket, temperature controller (Model TC-1000), and thermistor probe (YSI-451; IITC Life Science, Woodland Hills, CA, USA).

Fundus AF images (55° wide-field lens; 488-nm excitation; 0.98-mm detection pupil) were obtained with a cSLO (Spectralis HRA; Heidelberg Engineering, Heidelberg, Germany) with laser power set at approximately 280 μW and sensitivity at 95 to 100 after visual pigment was bleached for 20 seconds. Nine successive frames were acquired with the high-speed mode and frames were saved in non-normalized mode.

To quantify fundus autofluorescence (quantitative fundus AF [qAF]) the Spectralis was equipped with an internal fluorescence reference[28] to account for variations in laser power and detector sensitivity and focus was adjusted as previously published.[15] Using a dedicated image analysis program written in IGOR (Wavemetrics, Lake Oswego, OR, USA), mean gray levels (GL) were calculated from eight predefined segments around the optic disc (Fig. 1), blood vessels were excluded by histogram analysis, and qAF was calculated by normalization to the GL of the reference after subtraction of zero light (GL_0) and inclusion of a reference calibration factor.[15,28]

In fundus AF images, autofluorescent puncta were measured using the Spectralis image analysis tools. The transverse resolution of the laser scanning images is approximately 10 μm.[29]

Horizontal SD-OCT scans (1.8 mm) were also acquired with the Spectralis in high-resolution mode with averaging of 100 frames. A corneal radius of curvature of 1.22 was used after calibrating retinal thickness measurements in the SD-OCT scans to thicknesses at corresponding positions (0.2-mm intervals) in histological sections through the optic nerve head of four mice; the value used was consistent with previous determinations in mice.[30–34] Because axial length influences image magnification, distances from the base of the optic nerve to anterior cornea were measured in paraffin sections (10-μm thickness; ×20 magnification) at 3 and 6 months of age using Photoshop version 7 (Adobe Photosystems, Inc., San Jose, CA, USA). Measurements obtained in C57BL/6J (2.586 ± 0.034, mean ± SEM) and *Rdh8*$^{-/-}$*Abca4*$^{-/-}$ *(2.574 ± 0.018, mean ± SEM) mice (four eyes per group) were not significantly different (one-way ANOVA, $P > 0.05$).*

Histometric Analysis

Mouse eyes were fixed by immersion in 4% paraformaldehyde, 16.8% isopropyl alcohol, 2% trichloroacetic acid, and 2% zinc chloride in phosphate buffer for 24 hours at 4°C after marking the superior pole. Whole eyecups were embedded in paraffin and sectioned at a thickness of 8 μm. Sections were then counterstained using hematoxylin and eosin (H&E). Morphologic observations and light microscopy were performed using a digital imaging system (Leica Application Suite; Leica Microsystems, Welzlar, Germany). Outer nuclear layer (ONL) thickness was measured at 200-μm intervals superior and inferior to the edge of the optic nerve head (ONH) along the vertical meridian.[27] The section most centrally located within the ONH was used for measurements after imaging with a digital imaging system (×20 objective; Leica Microsystems); composite images were then created in Photoshop CS5. Serial H&E-stained sagittal sections were also collected from entire mouse eyes and stained to examine for structure changes and rearrangement of photoreceptor cells. The ONL area was also calculated as the sum of the ONL thicknesses in superior and

Investigative Ophthalmology & Visual Science

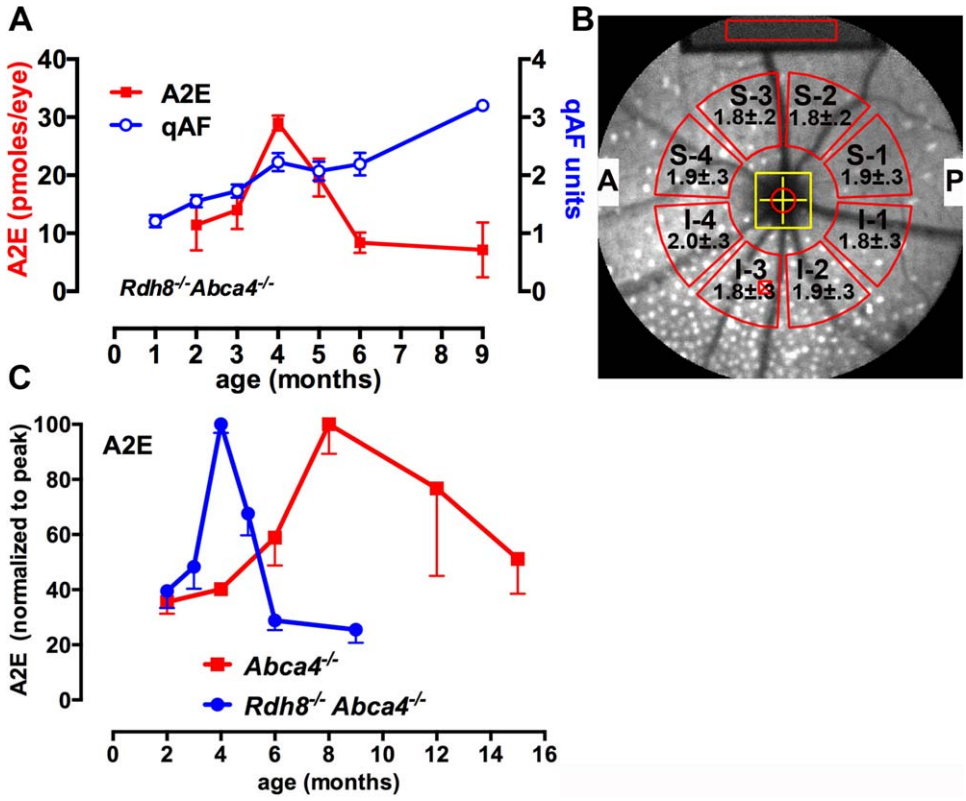

Figure 1. Quantitation by HPLC of bisretinoid lipofuscin and qAF in *Rdh8*$^{-/-}$*Abca4*$^{-/-}$ and *Abca4*$^{-/-}$ mice. (**A**) The A2E quantified in *Rdh8*$^{-/-}$*Abca4*$^{-/-}$ mice by reverse-phase HPLC (left *y*-axis) and qAF (right *y*-axis) are plotted as a function of age. The A2E values are mean ± SEM; A2E: four eyes per sample and two to six samples per mean; qAF: 12 to 15 mice at ages 1 to 6 months and 1 mouse at age 9 months. (**B**) The qAF values in *Rdh8*$^{-/-}$*Abca4*$^{-/-}$ mice were calculated as the average of the eight segments outlined in *red*. The eight segments are located between 8.25° and 19.25° from the center of the optic disc (*yellow cross*). The gray levels in each segment are normalized to values determined for the internal fluorescent reference (*top*); sampling area in the reference is indicated by the *red rectangle*. Superior (S-1–4) and inferior (I-1–4) segments are labeled: A, anterior; P, posterior. Values presented in each segment are qAF ± SEM (right eyes of eight mice, age 4 months). (**C**). High-performance liquid chromatography quantitation of A2E in *Rdh8*$^{-/-}$*Abca4*$^{-/-}$ and *Abca4*$^{-/-}$ mice are normalized to peak A2E levels (*Rdh8*$^{-/-}$*Abca4*$^{-/-}$: 4 months; *Abca4*$^{-/-}$ 8 months) and plotted as a function of age. Normalized mean ± SEM; four eyes per sample and two to six (*Rdh8*$^{-/-}$*Abca4*$^{-/-}$) or two to five (*Abca4*$^{-/-}$) samples per mean.

inferior retina (0.2–2.2 mm) and multiplied by the measurement interval of 0.2 mm.

Additionally, fixed eyes (1, 4, and 6 months) were mounted in Tissue-Tek OCT compound (Sakura Finetek, Torrance, CA, USA) and sectioned horizontally in a cryostat (15 µm). Sections through the ONH were stained with 4′,6-diamidino-2-phenylindole, dihydrochloride (DAPI) to label nuclei and were examined under a fluorescence microscope (×40 objective; Zeiss Axioplan II microscope with AxioCam HRc camera; Carl Zeiss, Thornwood, NY, USA) with DAPI (359/461 nm, excitation/emission maxima) and fluorescein (490/525) appropriate filter sets. The RPE lipofuscin has a broad yellow/orange emission (500–800 nm)[35]; with the 525-nm band-pass filter, a narrow spectral window of this emission is captured and the fluorescence is green.

Quantitative HPLC

The A2E and A2E-isomers were measured in mouse eyes (four eyes per sample) by HPLC (Alliance system; Waters Corp., Milford, MA, USA)[25] after homogenization and extraction in chloroform/methanol.[36] Absorbance peaks were identified by comparison with external standards. Molar quantities per eye were calculated from peak areas using standard concentrations determined spectrophotometrically together with published extinction coefficients, and by normalization to total sample volumes. Mean values for genotype and age were determined by averaging multiple independent samples.

Statistical Analyses

Analyses were performed using Prism 5 (GraphPad Software, La Jolla, CA, USA) and the statistical tests as indicated.

Results

Quantitative Fundus AF

Using a previously published approach,[15] we measured fundus AF levels in *Rdh8*$^{-/-}$*/Abca4*$^{-/-}$ mice from 1 to 9 months of age by calculating qAF values averaged over eight predetermined fundus segments (Figs. 1A, 1B). Measurements revealed an age-related increase in qAF, with the progressive increase in qAF being sustained from 1 to 9 months of age (oldest age studied) (Fig. 1B). The qAF coefficient of variation (CV) (SD/mean × 100) ranged from 25.5% (age 3 months) to 33.8% (age 1 month). The mean qAF values for the four superior (1.28 ± 0.11, $n = 15$; mean ± SEM) and four inferior segments (1.15 ± 0.10, $n = 15$; mean ± SEM) were normally distributed (D'Agostino and Pearson normality test) but the differences between the means at 1 month (superior: 1.28 ± 0.11; inferior: 1.15 ± 0.11; mean ± SEM; $n = 15$), 2 months (superior: 1.54 ± 0.10; inferior: 1.56 ± 0.11; mean

± SEM; $n = 15$), and 3 months (superior: 1.65 ± 0.10; inferior: 1.78 ± 0.13; mean ± SEM; $n = 15$) were not significant ($P > 0.05$, unpaired *t*-test).

Quantitation of Bisretinoids by HPLC

In eyes obtained from *Rdh8*$^{-/-}$/*Abca4*$^{-/-}$ mice, A2E, one of the bisretinoid constituents of RPE lipofuscin, was measured at various ages by integrating HPLC peak areas and normalizing to standard samples of known concentration. For comparison, we plotted the A2E dataset on the left *y*-axis of Figure 1A, with qAF displayed on the right *y*-axis. Although qAF exhibited an increasing trend from 1 to 9 months of age, A2E levels increased between 2 and 4 months of age and decreased thereafter. To contrast the profile of A2E accumulation in *Rdh8*$^{-/-}$/*Abca4*$^{-/-}$ mice with that in *Abca4*$^{-/-}$ mice, we also plotted previously published data[15] for A2E accumulation in *Abca4*$^{-/-}$ mice along with the data for *Rdh8*$^{-/-}$/*Abca4*$^{-/-}$ mice (Fig. 1C). As shown in Figure 1C, in both *Abca4*$^{-/-}$ and *Rdh8*$^{-/-}$/*Abca4*$^{-/-}$ mice,[25,37] A2E levels increased between 2 and 4 months of age but the rate of increase was greater in the *Rdh8*$^{-/-}$/*Abca4*$^{-/-}$ mice (Fig. 1A). Specifically, the slopes (±SEM) of the regression lines for *Abca4*$^{-/-}$ and *Rdh8*$^{-/-}$/*Abca4*$^{-/-}$ mice were 10.3 ± 2.3 (goodness of fit, R^2, 0.62) and 27.6 ± 6.2 (goodness of fit, R^2, 0.71), respectively. In *Rdh8*$^{-/-}$/*Abca4*$^{-/-}$ mice, A2E levels peaked at 4 months of age, whereas in *Abca4*$^{-/-}$ mice, the maximum occurred at 8 months of age.

Thickness of ONL

We measured ONL thickness as an indicator of photoreceptor cell viability in *Rdh8*$^{-/-}$/*Abca4*$^{-/-}$ mice and plotted thicknesses in 200-μm intervals superior and inferior to the ONH in the vertical plane (Fig. 2A). Differences between *Rdh8*$^{-/-}$/*Abca4*$^{-/-}$ and wild-type (C57BL/6N) (age 8 months) mice were readily visible, particularly in the superior hemisphere of retina. Thinning of ONL in *Rdh8*$^{-/-}$/*Abca4*$^{-/-}$ mice continued to progress from 3 to 6 months of age (Figs. 2A, 2B). For comparative purposes, we calculated ONL area from the sum of ONL thicknesses in superior and inferior retina (0.2 to 2.2 mm), multiplied by the measurement interval of 0.2 mm. Relative to the wild-type C57BL/6N mice (2.3×10^5 mm^2 ± 0.01, mean ± SEM) mean ONL area in 2-month-old (2.0×10^5 mm^2 ± 0.06) and 4-month-old (1.8×10^5 mm^2 ± 0.03) *Rdh8*$^{-/-}$/*Abca4*$^{-/-}$ mice was reduced by 11% and 21%, respectively. At 6 months of age, mean ONL area (1.4×10^5 mm^2 ± 0.02) was diminished by 40% ($P < 0.05$; nonparametric Kruskal-Wallis and Dunn's multiple comparison test). In C57BL/6N mice, ONL thicknesses were not different at 3, 6, and 8 months (data not shown).

Autofluorescence in Retinal Laminae

To better understand sources of fundus AF in *Rdh8*$^{-/-}$/*Abca4*$^{-/-}$ mice, we also examined cryostat sections of *Rdh8*$^{-/-}$/*Abca4*$^{-/-}$ mouse retinae in areas of normal lamination (Fig. 3). An inherent autofluorescence was observed not only in RPE cells, as expected, but also in the lamina occupied by photoreceptor outer segments. This autofluorescence in the *Rdh8*$^{-/-}$/*Abca4*$^{-/-}$ mice was more pronounced in older mice.

In Vivo and Ex Vivo Imaging of Autofluorescent Puncta

In fundus AF images, the *Rdh8*$^{-/-}$/*Abca4*$^{-/-}$ mice exhibited readily detectable AF spots predominantly in the inferior-nasal quadrant of the eye (Figs. 1E, 4, 5A, 5B). Measurements of the AF puncta in fundus images were acquired at 2, 4, and 6 months of age (two mice, 15 puncta per retina at each age). The mean diameter of the AF puncta was 30 μm (±0.96, SEM; range, 20–50 μm; sample size, 90). The data were normally distributed (D'Agostino & Pearson omnibus normality test) and no differences were observed among the age groups (one-way ANOVA, $P > 0.05$). Puncta of intense AF were only occasionally observed at 1 month of age, were increased in number between 3 and 5 months of age, and had diminished in frequency at 7 months of age (Fig. 4). In C57BL/6J mice, autofluorescent puncta were not observed at these ages (data not shown).

Spectral-domain OCT images of *Rdh8*$^{-/-}$/*Abca4*$^{-/-}$ mouse retinae were acquired at 2 to 8 months of age (Fig. 5C). In these images, the laminar organization of the retina was often interrupted by areas of abnormal outer retinal hyperreflectivity. These foci extended through the ONL and outer plexiform layer (OPL)-attributable reflectivity bands.

Histological analyzes were performed using H&E-stained paraffin sections of mouse retina at 1 to 6 months of age. Under the light microscope, the laminar arrangement of retina was often distorted by outer retinal folds and rosette-like structures (Figs. 5D, 5E). These aberrations involved a spherical organization of photoreceptor cell nuclei that usually occupied the ONL, extended across the OPL, and could also encroach on the inner nuclear layer. The center of the rosettes appeared to be occupied by photoreceptor inner and outer segments. Measurement of rosettes (including nuclei and inner core) in the H&E-stained sections (×20 objective; sample size 13) revealed a mean height of 44.1 (± 0.07, SEM) and mean width of 35.6 μm (±0.7, SEM; width at half height; range, 29.2–74.5).

To observe for the presence of AF in the rosettes, we examined cryostat (horizontal) sections that had been stained with DAPI to label nuclei. As shown in Figures 5F through 5H, circularly arranged DAPI-stained nuclei were observed in the ONL and OPL. The cores of these circular figures were positioned in the OPL and exhibited an AF when viewed by fluorescence microscopy. The dimensions of the rosette (based on DAPI staining; Fig. 5F) were determined using the integrated measurement module of the microscopy (×40 objective) and were found to be 35.2 μm (horizontal) and 28.1 μm (vertical).

Autofluorescent puncta were found to also be prominent in inferior–anterior fundus of *Abca4*$^{-/-}$ mice (Fig. 5I) that do not carry the *Crb1*^{rd8} mutation. Thus, these aberrations are not only conferred by the *Crb1*^{rd8} mutation in *Rdh8*$^{-/-}$/*Abca4*$^{-/-}$ mice.

Discussion

Previous studies have shown that mice carrying a double knockout of *Rdh8*$^{-/-}$/*Abca4*$^{-/-}$ exhibit rapid accumulation of the bisretinoids A2E and all-*trans*-retinal dimer and early-onset photoreceptor cell degeneration.[16] Our findings are consistent with this earlier work. As compared with single knockout *Abca4*$^{-/-}$ (albino) mice at age 4 months, A2E levels in the pigmented *Rdh8/Abca4*$^{-/-}$ mice were more than 2-fold greater. Thinning in the ONL in the *Rdh8/Abca4*$^{-/-}$ mice also was detected at an earlier age (*Abca4*$^{-/-}$ at age 8 months; *Rdh8/Abca4*$^{-/-}$ at age 4 months). We cannot compare qAF levels in the *Abca4*$^{-/-}$ and *Rdh8/Abca4*$^{-/-}$ mice, because the former were albino and the latter were pigmented. Even in the presence of equal levels of RPE lipofuscin, the absence of melanin in the albino mice can be expected to confer higher qAF values due to reflected light.[38]

In *Rdh8/Abca4*$^{-/-}$ mice, a decline in levels of the bisretinoid lipofuscin fluorophore A2E coincided with photoreceptor cell loss as measured by ONL thickness. We previously found that A2E also declined in *Abca4*$^{-/-}$ mice,

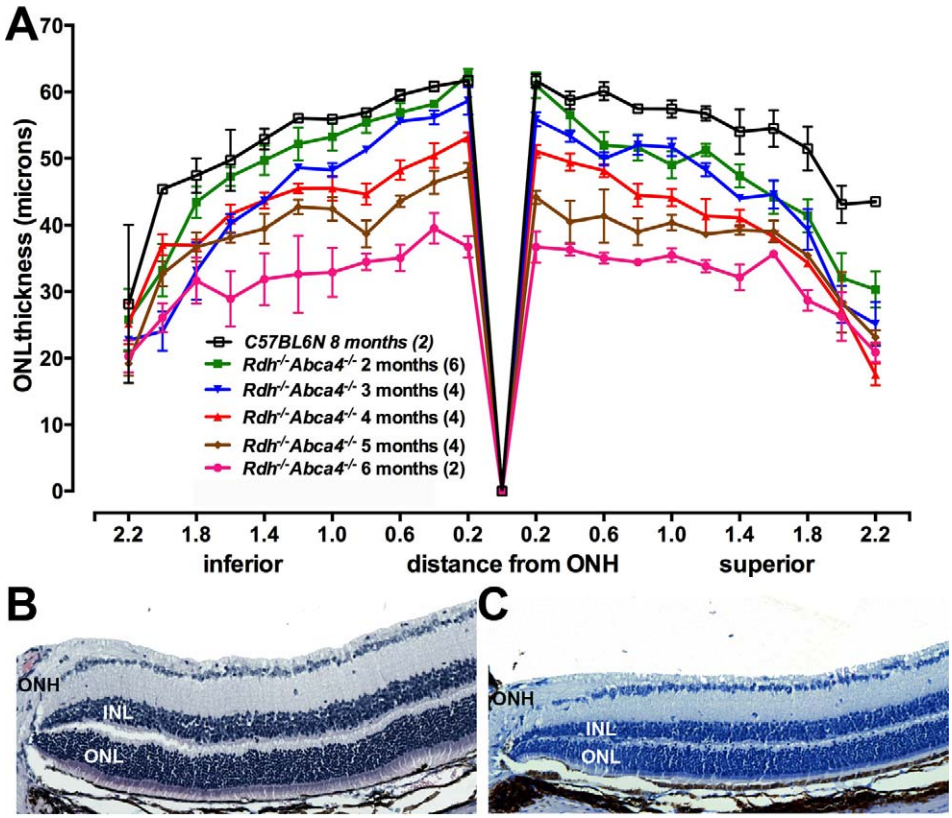

Figure 2. Outer nuclear layer thinning in *Rdh8*$^{-/-}$*/Abca4*$^{-/-}$ mice. (**A**) Quantification of ONL thickness in *Rdh8*$^{-/-}$*/Abca4*$^{-/-}$ (ages 2–6 months) and wild-type (C57BL/6N) mice (8 months), respectively. Means ± SEM are plotted as a function of distance from the ONH in the inferior and superior hemispheres. Numbers of mice are presented in parentheses. (**B**, **C**) Light micrographs of retinae of *Rdh8*$^{-/-}$*/Abca4*$^{-/-}$ mice at 2 (**B**) and 6 (**C**) months of age document progressive ONL thinning.

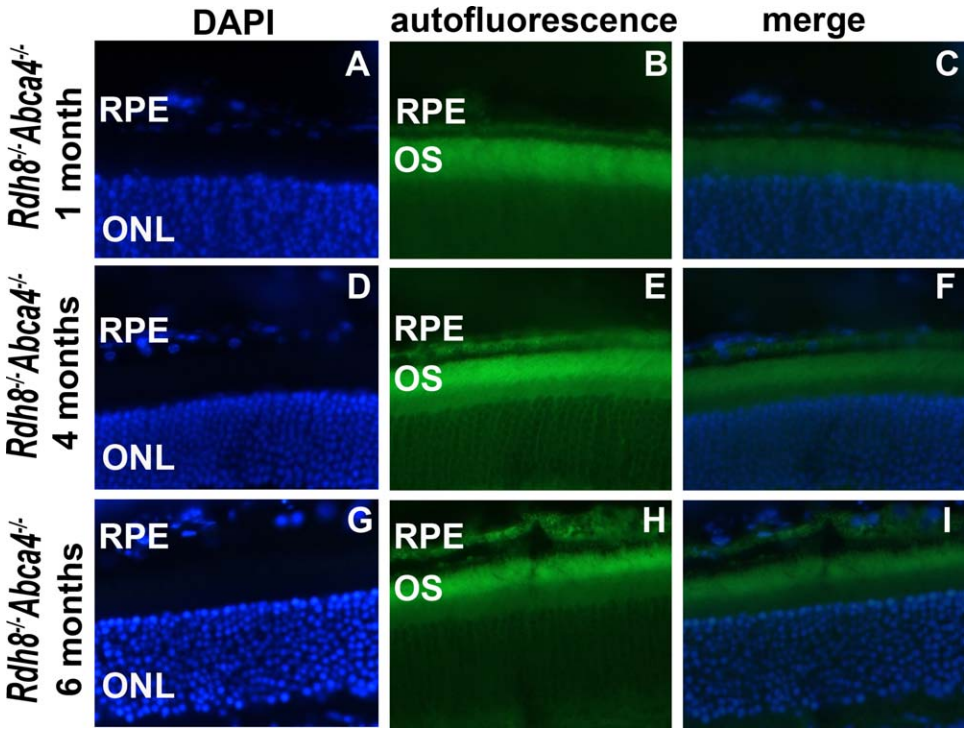

Figure 3. Fluorescence photomicrographs of mouse retina. *Rdh8*$^{-/-}$*Abca4*$^{-/-}$ mouse, age 1 month (**A**–**C**), age 4 months (**D**–**F**), and age 6 months (**G**–**I**). DAPI fluorescence, 7.4-ms exposure; autofluorescence (FITC-filter), 179-ms exposure.

Investigative Ophthalmology & Visual Science

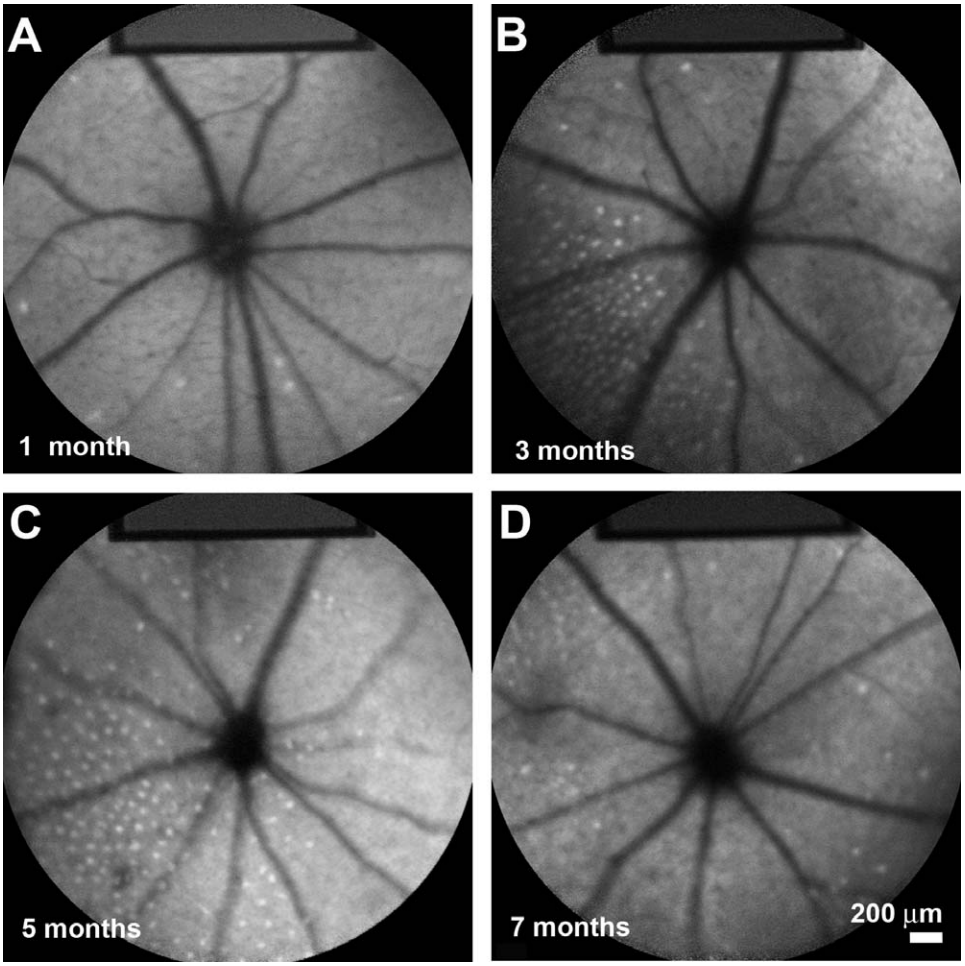

Figure 4. Fundus AF images of *Rdh8*$^{-/-}$*Abca4*$^{-/-}$ mice at the ages indicated. Left eyes. (**A**–**D**) Autofluorescence puncta emerge first in the inferior–anterior quadrant of the fundus and are also more abundant there.

concurrent with thinning of ONL.[15] Yet despite this decrease in bisretinoid, fundus AF continues to increase in both the *Abca4*$^{-/-}$[15] and *Rdh8/Abca4*$^{-/-}$ mice (Fig. 1). We formerly postulated that fundus AF can be potentiated in association with photoreceptor cell dysfunctioning and degeneration.[39,40] Perhaps, therefore, the continued increase in fundus AF observed after 4 months of age in *Rdh8/Abca4*$^{-/-}$ mice originates from the outer segments of degenerating photoreceptor cells. This notion is consistent with the age-related increase in AF observed in outer segments when viewed by fluorescence microscopy (Fig. 3). The identities of the specific fluorophores accounting for this continued increase in qAF are not yet known. Other bisretinoids potentially detectable by fundus AF could include A2PE, the precursor of A2E located in photoreceptor outer segments.[41] In this regard, two factors may enable the detection of fundus AF derived from photoreceptor cells positioned anterior to the RPE and allow this AF to appear particularly bright in pigmented *Rdh8/Abca4*$^{-/-}$ mice. First, the fluorescence emission from outer and inner segments would not be subject to absorbance by melanin as would be the case for lipofuscin in RPE. And second, although the fluorophores in the outer segments and perhaps inner segments of photoreceptor cells would presumably be present at lower concentrations, they also would be less compacted than in RPE cells and thus their fluorescence would undergo less self-absorption.

The background of the *Rdh8*$^{-/-}$*/Abca4*$^{-/-}$ mice we studied was complicated by the presence of the rd8 mutation in *Crb1*. Nonetheless, in our study of the features of AF in degenerating retina, we were able to use this complex phenotype to advantage. Retinae of both the *Rdh8*$^{-/-}$*/Abca4*$^{-/-}$[16] (Figs. 4, 5) and *Crb1*^{rd8}*/Crb1*^{rd8} mutant mice[19] are described as having photoreceptor cell rosettes. Interestingly, patients with retinal degeneration due to CRB1 mutations also exhibit intraretinal hyperreflective lesions that the authors suggest could represent the rosettes observed in mice.[42]

Here we visualized photoreceptor cell rosettes in mice by SD-OCT and by H&E and DAPI staining of retina sections. Autofluorescence originating in the center of the rosettes was detected by fluorescence microscopy and as AF puncta visible in vivo with imaging by SLO. The rosettes observed here varied in size. Using the magnification bars provided in the figures, we confirmed that the size range in our study was similar to the range presented in earlier publications.[23,43,44]

In other mouse models of retinal degeneration, AF spots have been observed in images of flat-mounted retina or by cSLO. This feature is exemplified by *Ccl2/Cx3cr1* mice, wherein granular-like hyperautofluorescent lesions in fundus AF images have been shown to correspond to hyperreflective lesions in the ONL-attributable band in OCT scans and to circularly arranged ONL nuclei in histological sections.[23] In other cases, the AF has been attributed to microglial cells.[21,22] For instance, CD11c-positive activated microglia have been

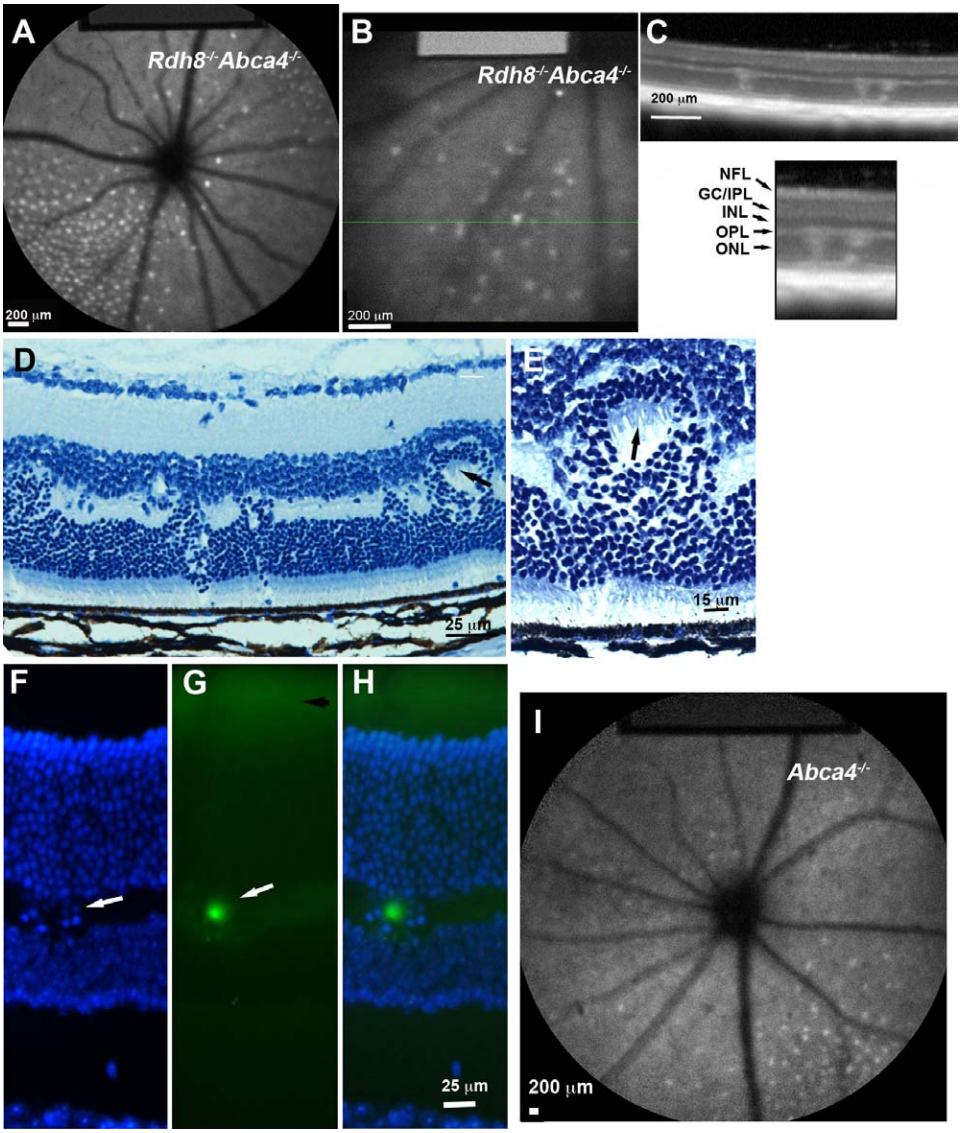

Figure 5. Multimodal imaging of retinae of *Rdh8*$^{-/-}$*Abca4*$^{-/-}$ and *Abca4*$^{-/-}$ mice. (**A**, **B**) Representative fundus AF (488-nm excitation) image of *Rdh8*$^{-/-}$*Abca4*$^{-/-}$ mouse (age 4 months; left eye) (**A**). Higher-magnification fundus AF image of inferior retina (age 5 months; left eye) (**B**). The *horizontal green line with arrow* indicates the position of the corresponding horizontal SD-OCT scan. (**C**) Spectral-domain OCT reveals hyperreflectivity extending through the ONL and IPL-attributable bands; *lower image* is region of the hyperreflectivity at higher magnification. GC/IPL, ganglion cell and inner plexiform layers; INL, inner nuclear layer; NFL, nerve fiber layer. (**D**, **E**) Light microscopic image of *Rdh8*$^{-/-}$*/Abca4*$^{-/-}$ mouse retina (age 3 months) stained with H&E. Rosette-like rearrangements of photoreceptor cells extend from ONL and across IPL toward INL. *Arrow*, photoreceptor outer segments project inward to form the core of the rosette. (**F**–**H**) Fluorescence micrographs of *Rdh8*$^{-/-}$*/Abca4*$^{-/-}$ retina (20-μm cryostat section). DAPI-stained nuclei (**F**); *white arrow*, nuclei of photoreceptor rosette extending from ONL through OPL. Inherently autofluorescent punctum (**G**) is observed in OPL using fluorescein (490/525) filter set. By merging images (**H**) of DAPI-stained nuclei (*blue*) with AF (*green*), it is clear that the AF is in the center of the rosette. (**I**) Fundus AF image of *Abca4*$^{-/-}$ mouse (age 8 months, right eye). Autofluorescence puncta are observed inferiorly.

identified in conjunction with disruptions in the ONL that present as photoreceptor cell rosettes.[17] Indeed, it has been suggested that in mice, although not in human retina, perivascular and subretinal microglia are the major lipofuscin-producing cells in normal aged mouse retina.[22] However, evidence based on fluorescence spectral profiles, age-associated accumulations, and disease relatedness indicates that fundus AF in mice originates primarily from lipofuscin in RPE cells, as is also the case in humans. For instance, in both humans and mice, RPE lipofuscin[37,45–48] and fundus AF[15,38,49,50] increase with age. Fundus AF and RPE lipofuscin both also increase with ABCA4 deficiency in humans[51,52] and mice.[53,54] The spectral characteristics of the fluorescence emission generated from RPE lipofuscin in mice also is similar to the fundus AF spectra recorded noninvasively in humans.[55,56] In a mouse retinal-detachment model, we found that autofluorescent puncta visible in the fundus exhibited emission spectra (emission peaks at 581 nm and 629 nm with excitations at 488 and 561 nm, respectively) that were consistent with an origin from the bisretinoid fluorophores that form in photoreceptor cell outer segments and become the constituents of RPE lipofuscin.[20] Moreover, the red-shift in emission maxima we recorded from the puncta at a longer (561 nm) versus shorter (488 nm) excitation wavelength was characteristic of the emission red-shifts observed for both fundus autofluorescence[35] and RPE lipofuscin.[56]

Of what significance are these findings? Fundus AF images obtained in humans presenting with some retinal diseases exhibit autofluorescent puncta. These disorders include central serous chorioretinopathy,[57] fundus albipunctatus,[58] and rod-cone degeneration caused by homozygous mutations in nuclear receptor transcription factor *NR2E3*.[21] In the latter case, it is suggested that these hyperautofluorescent spots correspond spatially to rosette-like photoreceptor cell rearrangements demonstrable by OCT. Nonetheless, the hyperautofluorescence of the puncta has been attributed to macrophage infiltration. Histopathologic studies of some cases of AMD and autosomal-dominant RP[24,59,60] have also documented photoreceptor cell rosettes. The lumina of the rosettes in both humans and mice have been shown to contain rhodopsin,[43,60] consistent with the presence of outer segments. In the rosettes described here, photoreceptor outer segments (OS) also extended into the center of the rosettes (Figs. 4, 5). Hyperreflective ovoid structures referred to as outer retinal tubulations[61,62] are observed in many forms of human retinal degeneration, including RP, Stargardt disease, and acute zonal occult outer retinopathy; these lesions are likely analogous to photoreceptor rosettes.

After considering published works together with our current findings, we conclude that autofluorescent puncta, observed in at least some mutant mouse lines, likely correspond to the outer segment–inhabited interior of photoreceptor cell rosettes, an abnormal feature of retinal disorders in both humans and mice. These findings do not preclude the possibility that microglial/macrophage cells are present in association with the rosettes; yet, we suggest that even given this eventuality, the AF is likely derived from outer-segment debris that has accumulated extracellularly or within macrophages after phagocytosis.

Our interest in undertaking this work was 2-fold. First, we wanted to further our understanding of fundus AF in relation to RPE lipofuscin accumulation and photoreceptor cell degeneration. Second, we aimed to determine whether photoreceptor cell rosettes/tubulations emit an AF. Common to both of these issues is the question of whether photoreceptor cells can contribute to aberrations in fundus AF. Based on our evidence of ONL thinning, the photoreceptor cells in the *Rdh8*$^{-/-}$/*Abca4*$^{-/-}$ mice are dysfunctional and progressively nonviable. In addition to the evidence of photoreceptor cell dysfunctioning based on diminishing numbers of nuclei in the ONL, fluorescence microscopy revealed that OS in the *Rdh8*$^{-/-}$/*Abca4*$^{-/-}$ mice exhibit a readily detectable AF that increased with age. Due to outer segment turnover,[63] bisretinoids do not normally accumulate in photoreceptor cells; thus we suggest that the increased AF in OS reflects dysfunctioning and degenerating photoreceptor cells. Mishandling of all-*trans*-retinal due to deficiency in *Rdh8* and *Abca4* would rapidly amplify bisretinoid formation in photoreceptor cells, leading to increased fundus AF intensity.[39] We also found that the interior of rosettes, a space occupied by photoreceptor inner and outer segments, was associated with an AF that was considerably brighter than the AF of surrounding puncta-free retina. Rosette formation undoubtedly disrupts the normal interface between OS and the apical domain of RPE, a relationship essential to daily photoreceptor maintenance (phagocytosis, retinoid exchange, nutrient exchange). Whether the AF intensity here is simply attributable to an accumulation of unphagocytosed outer segment membrane or whether the photoreceptor cells forming the rosette are subject to accelerated production of bisretinoid, is uncertain. Nonetheless, taken together, these findings illustrate that photoreceptor cells can serve as an abnormal source of heightened fundus AF. These findings also may be relevant to our understanding of the paracentral rings of elevated AF in retinitis pigmentosa[64] and/or the bright AF flecks that characterize recessive Stargardt disease.[51,65]

Acknowledgments

Supported by National Institutes of Health Grants RO1EY12951 and P30EY019007, Foundation Fighting Blindness, and by a grant from Research to Prevent Blindness to the Department of Ophthalmology, Columbia University. Also acknowledged is the Department of Veterans Affairs, Veterans Health Administration, Office of Research and Development, Biomedical Laboratory Research and Development Program through Veterans Administration Merit Award 1I01BX000669-01 (JMS), and an unrestricted grant from Research to Prevent Blindness to the Department of Ophthalmology (Ross Eye Institute), University at Buffalo-SUNY. The contents do not represent the views of the Department of Veterans Affairs or the US government. JMS is a member of the SUNY Eye Institute.

Disclosure: **E. Flynn**, None; **K. Ueda**, None; **E. Auran**, None; **J.M. Sullivan**, None; **J.R. Sparrow**, None

References

1. Sun H, Nathans J. Stargardt's ABCR is localized to the disc membrane of retinal rod outer segments. *Nat Genet*. 1997;17:15–16.
2. Illing M, Molday LL, Molday RS. The 220-kDa rim protein of retinal rod outer segments is a member of the ABC transporter superfamily. *J Biol Chem*. 1997;272:10303–10310.
3. Molday LL, Rabin AR, Molday RS. ABCR expression in foveal cone photoreceptors and its role in Stargardt macular dystrophy. *Nat Genet*. 2000;25:257–258.
4. Sullivan JM. Focus on molecules: ABCA4 (ABCR)—an import-directed photoreceptor retinoid flipase. *Exp Eye Res*. 2009;89:602–603.
5. Palczewski K, Jager S, Buczylko J, et al. Rod outer segment retinol dehydrogenase: substrate specificity and role in phototransduction. *Biochemistry*. 1994;33:13741–13750.
6. Haeseleer F, Jang GF, Imanishi Y, et al. Dual-substrate specificity short chain retinol dehydrogenases from the vertebrate retina. *J Biol Chem*. 2002;277:45537–45546.
7. Rattner A, Smallwood PM, Nathans J. Identification and characterization of all-trans-retinol dehydrogenase from photoreceptor outer segments, the visual cycle enzyme that reduces all-trans-retinal to all-trans-retinol. *J Biol Chem*. 2000;275:11034–11043.
8. Chen C, Thompson DA, Koutalos Y. Reduction of all-trans-retinal in vertebrate rod photoreceptors requires the combined action of RDH8 and RDH12. *J Biol Chem*. 2012;287:24662–24670.
9. Maeda A, Maeda T, Imanishi Y, et al. Role of photoreceptor-specific retinol dehydrogenase in the retinoid cycle in vivo. *J Biol Chem*. 2005;280:18822–18832.
10. Maeda A, Golczak M, Maeda T, Palczewski K. Limited roles of Rdh8, Rdh12, and Abca4 in all-trans-retinal clearance in mouse retina. *Invest Ophthalmol Vis Sci*. 2009;50:5435–5443.
11. Perrault I, Hanein S, Gerber S, et al. Retinal dehydrogenase 12 (RDH12) mutation in leber congenital amaurosis. *Am J Hum Genet*. 2004;75:639–646.
12. Janecke AR, Thompson DA, Utermann G, et al. Mutations in RDH12 encoding a photoreceptor cell retinol dehydrogenase cause childhood-onset severe retinal dystrophy. *Nat Genet*. 2004;36:850–854.
13. Chrispell JD, Feathers KL, Kane MA, et al. Rdh12 activity and effects on retinoid processing in the murine retina. *J Biol Chem*. 2009;284:21468–21477.
14. Maeda A, Maeda T, Sun W, Zhang H, Baehr W, Palczewski K. Redundant and unique roles of retinol dehydrogenases in the

mouse retina. *Proc Natl Acad Sci U S A*. 2007;104:19565–19570.

15. Sparrow JR, Blonska A, Flynn E, et al. Quantitative fundus autofluorescence in mice: correlation with HPLC quantitation of RPE lipofuscin and measurement of retina outer nuclear layer thickness. *Invest Ophthalmol Vis Sci*. 2013;54:2812–2820.
16. Maeda A, Maeda T, Golczak M, Palczewski K. Retinopathy in mice induced by disrupted all-trans-retinal clearance. *J Biol Chem*. 2008;283:26684–26693.
17. Chen X, Kezic J, Bernard C, McMenamin PG. Rd8 mutation in the Crb1 gene of CD11c-eYFP transgenic reporter mice results in abnormal numbers of CD11c-positive cells in the retina. *J Neuropathol Exp Neurol*. 2013;72:782–790.
18. Chakraborty D, Conley SM, Stuck MW, Naash MI. Differences in RDS trafficking, assembly and function in cones versus rods: insights from studies of C150S-RDS. *Hum Mol Genet*. 2010;19:4799–4812.
19. Mehalow AK, Kameya S, Smith RS, et al. CRB1 is essential for external limiting membrane integrity and photoreceptor morphogenesis in the mammalian retina. *Hum Mol Genet*. 2003;12:2179–2189.
20. Secondi R, Kong J, Blonska AM, Staurenghi G, Sparrow JR. Fundus autofluorescence findings in a mouse model of retinal detachment. *Invest Ophthalmol Vis Sci*. 2012;53:5190–5197.
21. Wang NK, Fine HF, Chang S, et al. Cellular origin of fundus autofluorescence in patients and mice with a defective *NR2E3* gene. *Br J Ophthalmol*. 2009;93:1234–1240.
22. Xu H, Chen M, Manivannan A, Lois N, Forrester JV. Age-dependent accumulation of lipofuscin in perivascular and subretinal microglia in experimental mice. *Aging Cell*. 2008;7:58–68.
23. Zhou Y, Sheets KG, Knott EJ, et al. Cellular and 3D optical coherence tomography assessment during the initiation and progression of retinal degeneration in the Ccl2/Cx3cr1-deficient mouse. *Exp Eye Res*. 2011;93:636–648.
24. Dunaief JL, Dentchev T, Ying GS, Milam AH. The role of apoptosis in age-related macular degeneration. *Arch Ophthalmol*. 2002;120:1435–1442.
25. Kim SR, Fishkin N, Kong J, Nakanishi K, Allikmets R, Sparrow JR. The Rpe65 Leu450Met variant is associated with reduced levels of the RPE lipofuscin fluorophores A2E and iso-A2E. *Proc Natl Acad Sci U S A*. 2004;101:11668–11672.
26. Mattapallil MJ, Wawrousek EF, Chan CC, et al. The Rd8 mutation of the Crb1 gene is present in vendor lines of C57BL/6N mice and embryonic stem cells, and confounds ocular induced mutant phenotypes. *Invest Ophthalmol Vis Sci*. 2012;53:2921–2927.
27. Wu L, Nagasaki T, Sparrow JR. Photoreceptor cell degeneration in *Abcr*$^{-/-}$ mice. *Adv Exp Med Biol*. 2010;664:533–539.
28. Delori FC, Greenberg JP, Woods RL, et al. Quantitative measurements of autofluorescence with the scanning laser ophthalmoscope. *Invest Ophthalmol Vis Sci*. 2011;52:9379–9390.
29. Paques M, Simonutti M, Roux MJ, et al. High resolution fundus imaging by confocal scanning laser ophthalmoscopy in the mouse. *Vision Res*. 2006;46:1336–1345.
30. Tkatchenko TV, Shen Y, Tkatchenko AV. Analysis of postnatal eye development in the mouse with high-resolution small animal magnetic resonance imaging. *Invest Ophthalmol Vis Sci*. 2010;51:21–27.
31. Schippert R, Burkhardt E, Feldkaemper M, Schaeffel F. Relative axial myopia in Egr-1 (ZENK) knockout mice. *Invest Ophthalmol Vis Sci*. 2007;48:11–17.
32. Schmucker C, Schaeffel F. A paraxial schematic eye model for the growing C57BL/6 mouse. *Vision Res*. 2004;44:1857–1867.
33. Zhou X, Shen M, Xie J, et al. The development of the refractive status and ocular growth in C57BL/6 mice. *Invest Ophthalmol Vis Sci*. 2008;49:5208–5214.
34. Chou TH, Kocaoglu OP, Borja D, et al. Postnatal elongation of eye size in DBA/2J mice compared with C57BL/6J mice: in vivo analysis with whole-eye OCT. *Invest Ophthalmol Vis Sci*. 2011;52:3604–3612.
35. Delori FC, Keilhauer C, Sparrow JR, Staurenghi G. Origin of fundus autofluorescence. In: Holz FG, Schmitz-Valckenberg S, Spaide RF, Bird AC, eds. *Atlas of Fundus Autofluorescence Imaging*. Berlin: Springer-Verlag; 2007:17–29.
36. Sparrow JR, Kim SR, Wu Y. Experimental approaches to the study of A2E, a bisretinoid lipofuscin chromophore of retinal pigment epithelium. *Method Mol Biol*. 2010;652:315–327.
37. Mata NL, Weng J, Travis GH. Biosynthesis of a major lipofuscin fluorophore in mice and humans with ABCR-mediated retinal and macular degeneration. *Proc Natl Acad Sci U S A*. 2000;97:7154–7159.
38. Charbel Issa P, Singh MS, Lipinski DM, et al. Optimization of in vivo confocal autofluorescence imaging of the ocular fundus in mice and its application to models of human retinal degeneration. *Invest Ophthalmol Vis Sci*. 2012;53:1066–1075.
39. Sparrow JR, Yoon K, Wu Y, Yamamoto K. Interpretations of fundus autofluorescence from studies of the bisretinoids of retina. *Invest Ophthalmol Vis Sci*. 2010;51:4351–4357.
40. Gelman R, Chen R, Blonska A, Barile G, Sparrow JR. Fundus autofluorescence imaging in a patient with rapidly developing scotoma. *Retin Cases Brief Rep*. 2012;6:345–348.
41. Ben-Shabat S, Parish CA, Vollmer HR, et al. Biosynthetic studies of A2E, a major fluorophore of RPE lipofuscin. *J Biol Chem*. 2002;277:7183–7190.
42. Aleman TS, Cideciyan AV, Aguirre GK, et al. Human CRB1-associated retinal degeneration: comparison with the rd8 Crb1-mutant mouse model. *Invest Ophthalmol Vis Sci*. 2011;52:6898–6910.
43. Conley SM, Stuck MW, Burnett JL, et al. Insights into the mechanisms of macular degeneration associated with the R172W mutation in RDS. *Hum Mol Genet*. 2014;23:3102–3114.
44. Wenzel A, von Lintig J, Oberhauser V, Tanimoto N, Grimm C, Seeliger MW. RPE65 is essential for the function of cone photoreceptors in NRL-deficient mice. *Invest Ophthalmol Vis Sci*. 2007;48:534–542.
45. Wing GL, Blanchard GC, Weiter JJ. The topography and age relationship of lipofuscin concentration in the retinal pigment epithelium. *Invest Ophthalmol Vis Sci*. 1978;17:601–607.
46. Feeney-Burns L, Hilderbrand ES, Eldridge S. Aging human RPE: morphometric analysis of macular, equatorial, and peripheral cells. *Invest Ophthalmol Vis Sci*. 1984;25:195–200.
47. Weiter JJ, Delori FC, Wing GL, Fitch KA. Retinal pigment epithelial lipofuscin and melanin and choroidal melanin in human eyes. *Invest Ophthalmol Vis Sci*. 1986;27:145–151.
48. Kim SR, He J, Yanase E, et al. Characterization of dihydro-A2PE: an intermediate in the A2E biosynthetic pathway. *Biochem*. 2007;46:10122–10129.
49. Delori FC, Goger DG, Dorey CK. Age-related accumulation and spatial distribution of lipofuscin in RPE of normal subjects. *Invest Ophthalmol Vis Sci*. 2001;42:1855–1866.
50. Greenberg JP, Duncker T, Woods RL, Smith RT, Sparrow JR, Delori FC. Quantitative fundus autofluorescence in healthy eyes. *Invest Ophthalmol Vis Sci*. 2013;54:5685–5693.
51. Eagle RC, Lucier AC, Bernardino VB, Yanoff M. Retinal pigment epithelial abnormalities in fundus flavimaculatus. *Ophthalmology*. 1980;87:1189–1200.
52. Delori FC, Staurenghi G, Arend O, Dorey CK, Goger DG, Weiter JJ. In vivo measurement of lipofuscin in Stargardt's

Investigative Ophthalmology & Visual Science

disease—fundus flavimaculatus. *Invest Ophthalmol Vis Sci*. 1995;36:2327–2331.

53. Weng J, Mata NL, Azarian SM, Tzekov RT, Birch DG, Travis GH. Insights into the function of Rim protein in photoreceptors and etiology of Stargardt's disease from the phenotype in abcr knockout mice. *Cell*. 1999;98:13–23.
54. Kim SR, Jang YP, Jockusch S, Fishkin NE, Turro NJ, Sparrow JR. The all-trans-retinal dimer series of lipofuscin pigments in retinal pigment epithelial cells in a recessive Stargardt disease model. *Proc Natl Acad Sci U S A*. 2007;104:19273–19278.
55. Sparrow JR, Gregory-Roberts E, Yamamoto K, et al. The bisretinoids of retinal pigment epithelium. *Prog Retin Eye Res*. 2012;31:121–135.
56. Sparrow JR, Wu Y, Nagasaki T, Yoon KD, Yamamoto K, Zhou J. Fundus autofluorescence and the bisretinoids of retina. *Photochem Photobiol Sci*. 2010;9:1480–1489.
57. Yamamoto K, Zhou J, Hunter JJ, Williams DR, Sparrow JR. Toward an understanding of bisretinoid autofluorescence bleaching and recovery. *Invest Ophthalmol Vis Sci*. 2012;53:3536–3544.
58. Genead MA, Fishman GA, Lindeman M. Spectral-domain optical coherence tomography and fundus autofluorescence characteristics in patients with fundus albipunctatus and retinitis punctata albescens. *Ophthalmic Genet*. 2010;31:66–72.
59. Milam AH, Jacobson SG. Photoreceptor rosettes with blue cone opsin immunoreactivity in retinitis pigmentosa. *Ophthalmology*. 1990;97:1620–1631.
60. Tulvatana W, Adamian M, Berson EL, Dryja TP. Photoreceptor rosettes in autosomal dominant retinitis pigmentosa with reduced penetrance. *Arch Ophthalmol*. 1999;117:399–402.
61. Zweifel SA, Engelbert M, Laud K, Margolis R, Spaide RF, Freund KB. Outer retinal tubulation: a novel optical coherence tomography finding. *Arch Ophthalmol*. 2009;127:1596–1602.
62. Goldberg NR, Greenberg JP, Laud K, Tsang SH, Freund KB. Outer retinal tubulation in degenerative retinal disorders. *Retina*. 2013;33:1871–1876.
63. Bok D. Retinal photoreceptor-pigment epithelium interactions. Friedenwald lecture. *Invest Ophthalmol Vis Sci*. 1985;26:1659–1694.
64. Robson AG, Michaelides M, Luong VA, et al. Functional correlates of fundus autofluorescence abnormalities in patients with RPGR or RIMS1 mutations causing cone or cone rod dystrophy. *Br J Ophthalmol*. 2008;92:95–102.
65. Cukras CA, Wong WT, Caruso R, Cunningham D, Zein W, Sieving PA. Centrifugal expansion of fundus autofluorescence patterns in Stargardt disease over time. *Arch Ophthalmol*. 2012;130:171–179.

Investigative Ophthalmology & Visual Science